

DEFECT ACCUMULATION IN NANOPOROUS WEAR-RESISTANT COATINGS UNDER COLLECTIVE RECRYSTALLIZATION. SIMULATION BY HYBRID CELLULAR AUTOMATON METHOD

Dmitry D. Moiseenko¹, Pavel V. Maksimov², Sergey V. Panin³ and Viktor E. Panin⁴

^{1,2,3,4}Institute of Strength Physics and Materials Science SB RAS
634055, Akademichesky av. 2/4, Tomsk, Russia
e-mail: moisey@rocketmail.com¹, mpv@ispms.tsc.ru²

^{3,4}National Research Tomsk Polytechnic University
634050, Lenin av. 30, Tomsk, Russia
e-mail: svp@ispms.tsc.ru³, paninve@ispms.tsc.ru⁴

Keywords: wear-resistant coatings, cellular automata, recrystallization, thermal loading.

Abstract. *A modification of a multiscale hybrid discrete-continual approach of excitable cellular automata is developed. The new version of the method is completed by taking into account porosity and nanocrystalline structure of a material and the algorithms of calculation of local force moments and angular velocities of microrotations. The excitable cellular automata method was used to carry out numerical experiment (NE) for heating of continuous and nanoporous specimens consisting of nanocrystalline TiAlC coatings. The numerical experiments have shown that nanoporosity allows to substantially reducing the rate of collective crystallization. Nanoporosity slowed down propagation of the heat front in specimens. This fact can play both positive and negative roles in deposition of coating and its further use. On the one hand, by slowing the heat front propagation one can significantly reduce the level of thermal stresses in deeper layers of the material. On the other hand, such deceleration in case of the high value of the coefficient of thermal expansion can give rise to the formation of large gradients of thermal stress, which initiate nucleation and rapid growth of the main crack.*

1 INTRODUCTION

Currently, composite coatings on the basis of MAX phases with composite properties (tribological and heat-proof at the same time) become more and more relevant [1–7]. This new class of materials is characterized by unique properties combining the benefits of both metallic alloys and ceramic materials. On the one hand, such compounds demonstrate high heat conductivity and thermal resistance. On the other hand, they feature high elastic moduli, low thermal expansion coefficient, high heat resistance and extreme high-temperature strength. Such materials are very resistant to cycle loads and temperatures higher than 1000 °C, and in this temperature range their resistance to cycle loads leaves behind the majority of known heat-proof and heat-stable materials, including the intermetallide-based alloys [3].

The practical interest to such new materials is primarily connected with new requirements to critical units of aircraft. In combination with low density of the composite the unique characteristics of MAX-phases unveil wide range of their application in rocket and aircraft engineering. For instance, the implementation of heat-stable Ti-Al-based material with protective coating allows increasing up to 50% the relation of lift force to weight in comparison with the best Ni-based analogues [6].

However, the creation of new classes of wear resistant materials operating under extremely high temperature gradients (~1000 K) requires detailed study of both initial microstructure of created coatings and regulations of its evolution in the course of thermal and mechanical loads. For example, the melting temperature of γ -TiAl phase is about 1750 K, which limits the application of such intermetallides under extreme thermocycling.

Recent years have witnessed the works on modeling of either behavior of wear resistant and heat-proof coatings under mechanical loading [8, 9], or the process of their creation [10–11]. The majority of them is dedicated to the investigation of titanium-aluminum alloys. Unfortunately, the authors of present work are not aware of works that aim at detailed study of the change in the mesostructure of Ti-Al-C coatings under thermocycling at temperatures close to melting temperatures of separate structural elements. The capability of collective crystallization as well as its impact on redistribution of internal thermal stresses in a mesostructure are also far from being studied thoroughly.

Consequently, the authors of this work tried to implement computer modeling to study collective crystallization of nanostructured highly porous Ti-Al-C coating, as well as the effect of dynamic rearrangement of the structure on distribution of thermal stresses.

In the present work, the authors refer to the principles of physical mesomechanics on scale invariability assuming that a real solid body is an hierarchically organized system [12]. Such 3D-system contains the combination of interfaces, which are independent 2D-systems, in which rotary wave fluxes of mass and energy propagate [13]. Fig. 1 depicts the scheme of interaction of 2D planar subsystem of interface and 3D subsystem of the crystal lattice.

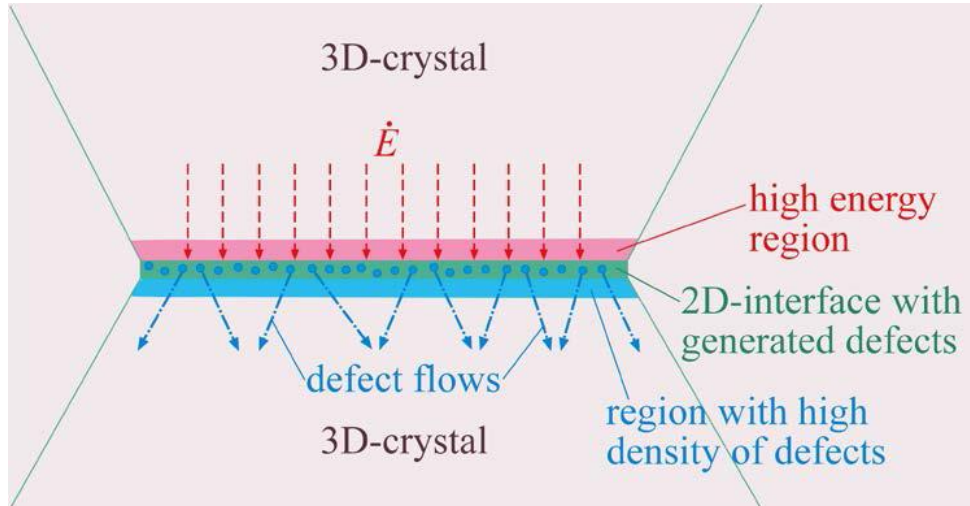


Fig. 1. Scheme of interaction of 2D planar subsystem of interface and 3D subsystem of the crystal lattice.

Rotary wave fluxes are particularly distinguished under dynamic loading, for instance under friction with run-out. Most distinctively the microrotations are demonstrated in experiments on fragmentation during propagation of a shock wave [14]. Rotation modes of deformation occur after the action of local moment of force. For computer modeling of the initiation and consequent evolution of fields of local force moments under intense dynamic loads, a discrete continuum method of stochastic excitable cellular automata was developed.

The authors were mostly referring to existing works on modeling of recrystallization processes [15–17] and to their own previous studies [18–20].

2 SIMULATION METHOD

Within the framework of present study, a new modification of the multiscale hybrid discrete continuum approach of stochastic excitable cellular automata was developed. The new method explicitly accounts for the porosity and nanocrystalline structure of material, the algorithm for computing local force moments and angular velocities of microrotations occurring in structurally nonuniform medium.

In the frame of SECA method (Stochastic Excitable Cellular Automata), the modeled specimen is represented as a cellular automaton, i.e. the combination of ordered active elements, each both imitating in part the material contained in particular volume of space and characterized by such numerical parameters as heat capacity and heat conductivity. The network of cellular automaton elements is divided into *clusters*, each being the model of a separate grain having its own orientation of the crystal lattice characterized by Euler angles ψ, φ, η .

To determine the temperature of the elements it was necessary to introduce a discrete model of heat transfer of heterogeneous medium. At zero step of the numerical experiment, for each element, the initial values of temperature, deformation, heat conductivity, heat capacity and coefficient of linear thermal expansion were assigned. Then, at each n -th time step, a new temperature value is calculated for an element with due consideration of heat fluxes from each adjacent element.

$$T_i^n = T_i^{n-1} + \frac{1}{c_i \rho_i V} \sum_{k=1}^N Q_{ik}^n, \quad (1)$$

where T_i^{n-1} , T_i^n are temperatures of the i -th element at $n-1$ and n -th time steps, c_i is heat capacity of the i -th element, ρ_i is the density of the i -th element, V is element volume, Q_{ik}^n is the flux of heat energy from neighboring k -th element into considered i -th at the n -th time step, N is the number of neighbors.

The change of heat energy Q_{ik}^n is calculated using Fourier law:

$$Q_{ik}^n = \frac{\lambda_{ik} \Omega}{l} (T_k^{n-1} - T_i^{n-1}) \Delta \tau. \quad (2)$$

Here λ_{ik} is the coefficient of mutual heat conductivity, l is the distance between the centers of considered elements, Ω is the area of adjacent plane, $\Delta \tau$ is time step. The coefficient of mutual heat conductivity is calculated as follows:

$$\lambda_{ik} = (\lambda_i + \lambda_k) / 2. \quad (3)$$

Here λ_i , λ_k are heat conductivity coefficients of the i -th and k -th elements, with

$$\lambda_j = \tilde{\lambda}_j e^{-\phi_j \theta_{jk}} \quad (j = i, k), \quad (4)$$

where $\tilde{\alpha}_j$ is the coefficient of heat conductivity of the j -th automaton, ϕ_j is the coefficient determining the fraction of impact of phonons on the material heat conductivity, u_{ik} is angle (in degrees) determined by the difference of crystal lattice orientations of i -th and k -th automata (in current program version $\theta_{jk} = |\phi_i - \phi_k|$).

After the calculation of new temperature values T_i^n using equation (1), for each i -th element the following values are calculated:

a. change in deformation due to thermal expansion:

$$\Delta_Q \xi_i^n = \alpha_f \cdot (T_i^n - T_i^{n-1}); \quad (5)$$

b. corresponding changes in stress and mechanical energy A_i^n :

$$\Delta_Q \sigma_i^n = \alpha_f \cdot (T_i^n - T_i^{n-1}) \cdot Y_i^n, \quad (6)$$

$$(7)$$

$$\Delta_Q A_i^n = \frac{Y_i^n \cdot V_{CA}}{2} \cdot \left(\text{sign}(\xi_i^{n-1} + \Delta_Q \xi_i^n) \cdot (\xi_i^{n-1} + \Delta_Q \xi_i^n)^2 - \text{sign}(\xi_i^{n-1}) \cdot (\xi_i^{n-1})^2 \right);$$

c. new values of heat energy Q_i^n :

$$(8)$$

$$Q_i^n = Q_i^{n-1} + c_i \cdot (T_i^n - T_i^{n-1}) - \Delta_Q A_i^n;$$

d. according to (8), a correction is made for a new temperature value:

$$T_i^n = T_i^{n-1} - \frac{\Delta Q A_i^n}{c_i}. \quad (9)$$

Thus, the fraction of element heat energy change goes for the change in its mechanical energy due to the process of thermal expansion. As a result, internal thermal stresses accumulate, which transform into fluxes of mechanical energy distributed long the network of elements.

The modeling of heat transfer in porous body should account the transfer of heat energy by radiation. In the frame of the considered method, a state of element is introduced that indicates its belonging to a pore. If the considered i -th automaton element on the first coordination sphere has an element in *pore* state, then the heat inflow into the i -th element is calculated from the assumption of cubic packing of elements, and that the pore boundaries are reflective, i.e. radiated and reflected rays propagate perpendicularly to the boundary. In this case, the neighboring element is the elements in *material* state that is the closest on the way of propagation of rays from the i -th element. Let this element have index k . The change in heat energy of the i -th element after the interaction with the k -th element at current n -th time step Q_{ik}^n is determined as follows.

In the case of radiant heat exchange, the i -th element, in addition to its generated radiation E_i^n , partially reflects the incident energy from the k -th element. The sum of energy of generated and reflected radiation is the effective radiation of the i -th element $(E_i^n)_{eff}$. For the calculation of the radiant heat exchange between elements, it is important to determine resulting radiation, which is the difference between the radiant flux received by an element and radiant flux which it radiates. To determine the flux density of the resulting radiation q_{ik}^n , an energy balance equation is composed:

$$q_{ik}^n = (E_i^n)_{eff} - (E_k^n)_{eff}. \quad (10)$$

On the other hand, the resulting radiation is the difference between the flux radiated by an element and the fraction of absorbed energy:

$$q_{ik}^n = E_i^n - \mu_i (E_k^n)_{eff}, \quad (11)$$

where $\mu_i \in [0;1]$ - is absorption coefficient of the i -th element. Taking into account (10) and (11) yields:

$$(E_i^n)_{eff} = q_{ik}^n \left(1 - \frac{1}{\mu_i}\right) + \frac{E_i^n}{\mu_i}. \quad (12)$$

To calculate the heat energy Q_{ik}^n transferred from the k -th element to the i -th one, a model of heat flux is used in a system of paralleled reflecting plates. In the frame of the model, using the principles of the law of radiant heat exchange, the equation for calculating the radiant heat exchange between elements can be derived. Let us derive the equation for determining heat flux q_{ik}^n from the k -th element to the i -th one. This value is the difference between effective fluxes from each of the elements:

$$q_{ik}^n = E_k^n - E_i^n. \quad (13)$$

Thus, according to (12) and taking into account that under stabilized regime, the resulting fluxes for each of the elements have equal value and opposite signs ($q_{ik}^n = -q_{ki}^n$):

$$\begin{aligned} (E_k^n)_{eff} &= -q_{ik}^n \left(1 - \frac{1}{\mu_k}\right) + \frac{E_k^n}{\mu_k}, \\ (E_i^n)_{eff} &= q_{ik}^n \left(1 - \frac{1}{\mu_i}\right) + \frac{E_i^n}{\mu_i}, \end{aligned} \quad (14)$$

where μ_i is the absorption coefficient of material of the i -th element. Substituting (14) into (13) yields the expression for heat flux q_{ik}^n :

$$q_{ik}^n = \frac{\mu_i \mu_k}{\mu_i + \mu_k - \mu_i \mu_k} \left[\frac{E_k^n}{\mu_k} - \frac{E_i^n}{\mu_i} \right]. \quad (15)$$

According to the laws of Stefan-Boltzmann and Kirchhoff, the relation of the flux density of heat energy E_i^n —radiated by the surface of heated i -th element containing material—to its absorption coefficient is calculated as follows:

$$\frac{E_i^n}{\mu_i} = \eta \left(\frac{T_i^n}{100} \right)^4. \quad (16)$$

Here $\eta = 5.67 \text{ W}/(\text{m}^2 \cdot \text{K}^4)$ is the radiation coefficient of gray body, μ_i is absorption coefficient of material of the i -th element, T_i^n - temperature of the i -th element at previous time step.

Obviously, the heat flux Q_{ik}^n over the time step $\Delta\tau$ through the element plane area Ω is expressed as:

$$Q_{ik}^n = q_{ik}^n \Omega \Delta\tau. \quad (17)$$

Taking into account (15) and (16) yields the expression for heat flux Q_{ik}^n :

$$Q_{ik}^n = \frac{\mu_i \mu_k}{\mu_i + \mu_k - \mu_i \mu_k} \eta \left[\left(\frac{T_k^n}{100} \right)^4 - \left(\frac{T_i^n}{100} \right)^4 \right] \Omega \Delta\tau. \quad (18)$$

Here, $\mu_i, \mu_k \in [0;1]$ - are absorption coefficients of the i -th and k -th elements.

Thus, the modeling of radiant heat exchange using (2) requires adding expression (18):

$$Q_{ik}^n = \frac{\lambda_{ik} \Omega}{l} (T_k^{n-1} - T_i^{n-1}) + \frac{\mu_i \mu_k}{\mu_i + \mu_k - \mu_i \mu_k} \eta \left[\left(\frac{T_k^n}{100} \right)^4 - \left(\frac{T_i^n}{100} \right)^4 \right] \Omega \Delta\tau. \quad (19)$$

Taking into account that the amount of radiated energy is known to be larger than the amount of energy absorbed by the walls of pores due to dissipation (connected with the absorption and dissipation coefficients), the energy dissipation during the heat transfer through

pores is expressed using optical thickness of gaseous filler of pores. Hence, coefficients μ_i and μ_k should be selected with the regard for the heat energy dissipation in the filler gas in pores. The chemical composition of the gas can be determined experimentally.

Further, due to heterogeneous thermal expansion, in different structural elements, internal thermal stresses accumulate that transform into fluxes of mechanical energy redistributed along the network of a cellular automaton. The method explicitly accounted grain boundaries, their curvature and grain-boundary angles of the crystal lattice. The created algorithms allowed calculating the value of local force moments, vorticity tensor and dissipation of torsion energy conditioned by the formation of new defect structures.

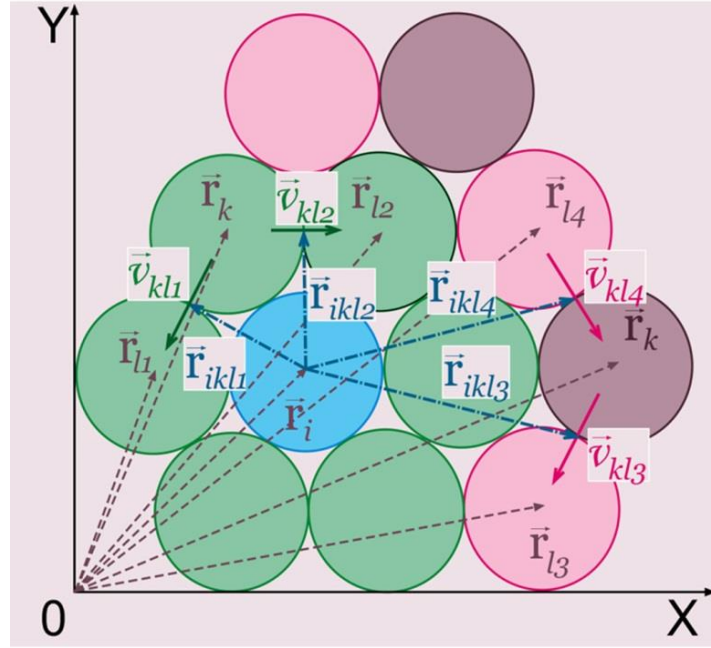


Fig. 2. Scheme for calculation of angular velocity of material rotation in cellular automaton element

Angular velocity of the i -th element in Fig. 2 under the flux of matter acting through the boundary of the k -th and l -th elements (each k -th element lies on the 1st coordination sphere of the i -th element; each l -th element lies on the intersection of 1st coordination spheres of the i -th and corresponding k -th elements) is calculated as follows:

$$\vec{\omega}_{ikl} = \frac{\vec{r}_{ikl} \times \vec{v}_{kl}}{|\vec{r}_{ikl}|^2}. \quad (20)$$

The velocity of matter flux at the boundary of the k -th and l -th elements is calculated using Newton's viscous flow equation:

$$\vec{v}_{kl} = m_{kl}(p_l - p_k)\vec{n}_{kl}, \quad (21)$$

where p_l , p_k are pressures (all-way stresses) in the k -th and l -th elements, \vec{n}_{kl} is vector of a normal to the boundary of the k -th and l -th elements, m_{kl} is movability of the boundary between the k -th and l -th elements.

The total angular velocity of the i -th element is determined as the following sum:

$$\vec{\omega}_i = \sum_{k=1}^K \sum_{l=1}^L \vec{\omega}_{ikl}. \quad (22)$$

Here K is the number of elements on 1st coordination sphere of the i -th element, L is the number of elements at the intersection of the 1st coordination spheres of the i -th element and each k -th neighbor.

Three-dimensional rotation angle of the i -th element over time τ ($\Delta\vec{\gamma}_i$) is proportional to the total angular velocity:

$$\Delta\vec{\gamma}_i = \vec{\omega}_i \tau. \quad (23)$$

Change of the force moment of the i -th element over time τ ($\Delta\vec{M}_i$) is calculated as follows:

$$\Delta\vec{M}_i = \frac{G\pi r_c^3 \Delta\vec{\gamma}_i}{2} = \frac{G\pi r_c^3 \vec{\omega}_i \tau}{2}. \quad (24)$$

Here G is shear modulus of material, contained in the i -th element, r_c is element radius. Vortex vector is determined as follows:

$$\vec{\omega}_i = \text{rot } \vec{v}. \quad (25)$$

Components of vortex vector are expressed as follows:

$$\begin{aligned} \omega_1 &= 2\Omega_{23}, \\ \omega_2 &= 2\Omega_{31}, \\ \omega_3 &= 2\Omega_{12}, \end{aligned} \quad (26)$$

where Ω is vorticity tensor,

$$\Omega_{ij} = \frac{1}{2} \left(\frac{\partial v_i}{\partial x_j} - \frac{\partial v_j}{\partial x_i} \right). \quad (27)$$

The meaning of angular velocity calculated using expressions 20–22 is similar to that of vortex vector. Taking into account equation 24, the following expressions for vortex vector components are yielded:

$$\begin{aligned} \omega_1 &= \frac{2M_1}{G\pi r_c^3 \tau}, \\ \omega_2 &= \frac{2M_2}{G\pi r_c^3 \tau}, \\ \omega_3 &= \frac{2M_3}{G\pi r_c^3 \tau}. \end{aligned} \quad (28)$$

Thus, vorticity tensor Ω can be expressed as follows:

$$\Omega = \begin{pmatrix} 0 & \frac{M_3}{G\pi r_c^3 \tau} & -\frac{M_2}{G\pi r_c^3 \tau} \\ -\frac{M_3}{G\pi r_c^3 \tau} & 0 & \frac{M_1}{G\pi r_c^3 \tau} \\ \frac{M_2}{G\pi r_c^3 \tau} & -\frac{M_1}{G\pi r_c^3 \tau} & 0 \end{pmatrix}. \quad (29)$$

The member responsible for accumulation of latent energy of defects is expressed in the following way:

$$\left[\Delta \vec{A}_d \right]_i^n = \frac{k_{tors} G_i |\Delta \vec{\gamma}_i^n| \pi r_c^3}{2} \Delta \vec{\gamma}_i^n. \quad (30)$$

Here, k_{tors} is the rate of accumulation of defects (can be determined experimentally).

It should be noted that expression (30) has general sense and, depending on formulated rules of switching of cellular automaton, can have the sense of energy required for reversible structure and phase transformation. In such a case, the coefficient k_{tors} can be calculated using atomic configurations of initial and final states.

3 NUMERICAL EXPERIMENT

In the frame of this work, theoretical study was performed of the character of structure and phase transformations in nanocrystalline and nanoporous specimens under thermocycling. The hybrid method of excitable and bistable cellular automata was used to simulate heat transfer with due account for the process of collective recrystallization.

Using the method of stochastic excitable cellular automata a numerical experiment (NE) was performed including the heat-up of solid and nanoporous specimens consisting of nanocrystalline TiAlC with high ($12 \cdot 10^{-6} \text{ K}^{-1}$) and low ($7 \cdot 10^{-6} \text{ K}^{-1}$) thermal expansion coefficient (TEC). The NE included the simulation of collective crystallization and thermal expansion of materials, as well as the explicit account for thermal transition of mechanical energy into its latent fraction during local rotations: at each time step, the mechanical energy of each element of a cellular automaton was decreasing for a value proportional to the square of absolute value of accumulated three-dimensional angle of rotation of this element.

Each specimen was simulated by means of a cellular automaton with fcc arrangement of elements with the dimensions of 60 nm. The dimensions of each element were $2.88 \times 2.4 \times 1.6 \text{ } \mu\text{m}$; the dimensions of grain and pore were set to 60 nm (Fig. 3). Initial temperature of each element was 300 K; initial values of deformation and stress were zero. The value of time step was 0.02 ns. Thermal loading consisted of two time steps of 1000 μs : at the first stage, heating up to upper limit of 1500 K was simulated; at the second stage, cooling to 300 K (Fig. 4).

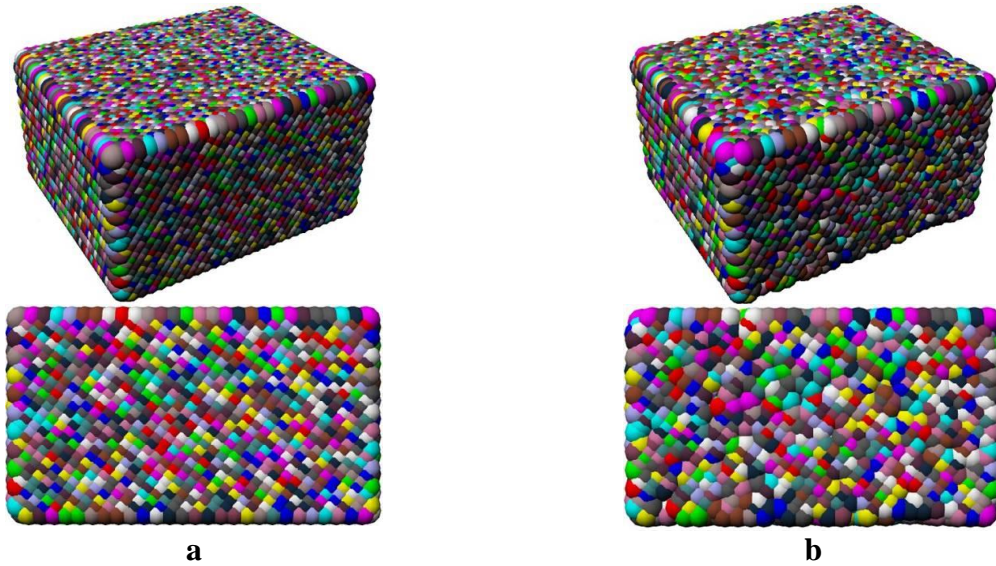


Fig. 3. Grain structure of specimens (in three-dimensional form and at the front face) at the initial moment of time: a) without pores with high and low TEC; b) porous with high and low TEC.

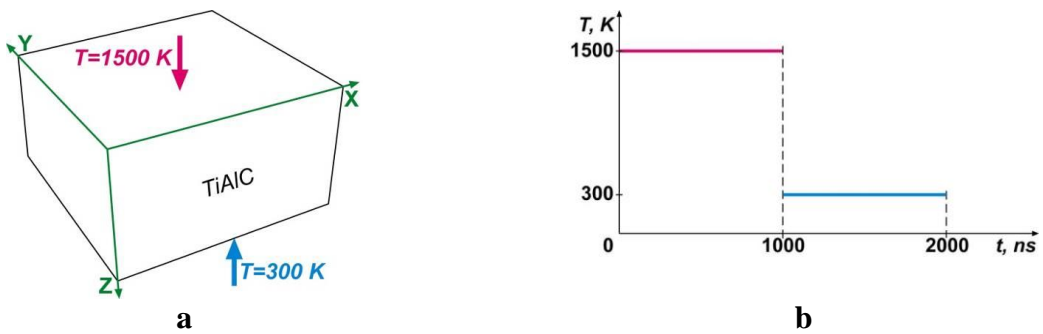


Fig. 4. Scheme of thermal load application (a) and time dependence of temperature at upper face (b)

Fig. 5 illustrates the images of grain structure of specimens (in three-dimensional form and at the front face), formed after collective crystallization by specific moment of time.

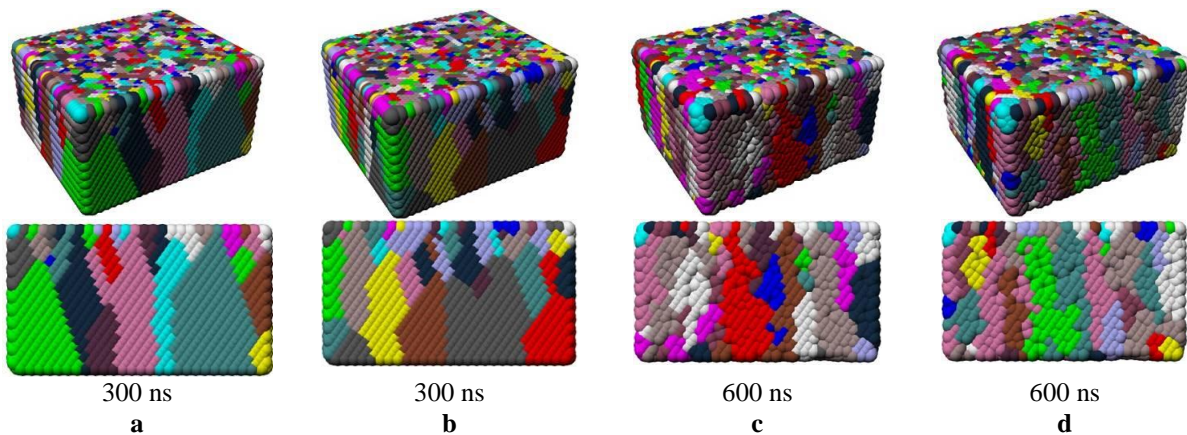


Fig. 5. Images of grain structure of specimens (in three-dimensional form and at the front face), formed after collective crystallization by specific moment of time: a) without pores with high TEC; b) without pores with low TEC; c) porous with high TEC; d) porous with low TEC.

Figs. 6–9 depict the time dependencies of mean values of effective stress, specific latent mechanical energy, relative latent mechanical energy and modulus of force moment at the stage of heating of the specimens.

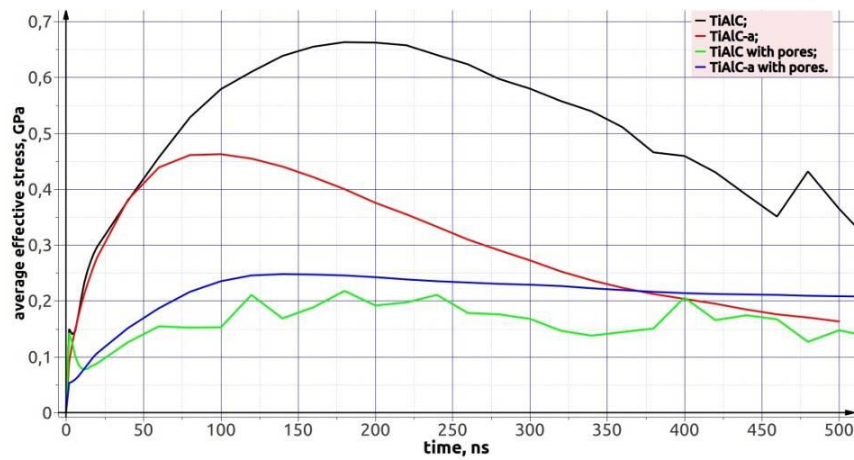


Fig. 6. Time plots of mean **effective stress** for specimens without pores with high TEC (black), without pores with low TEC (red), porous with high TEC (green), porous with low TEC (blue).

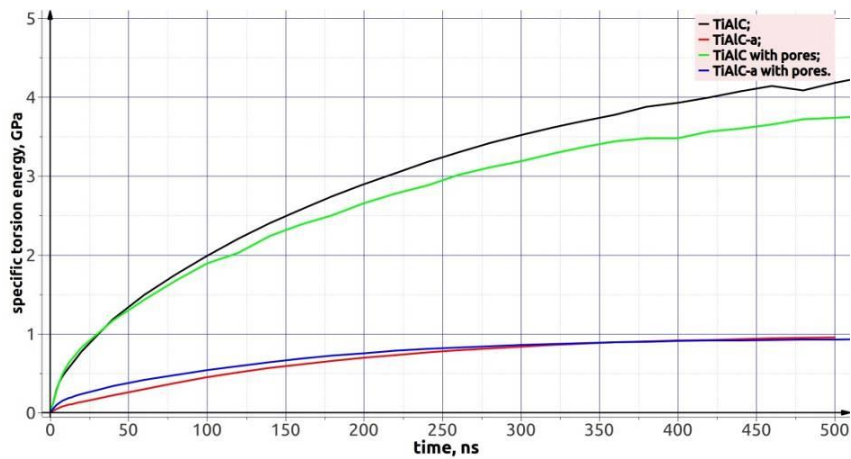


Fig. 7. Time plots of mean **specific latent mechanical energy** for specimens without pores with high TEC (black), without pores with low TEC (red), porous with high TEC (green), porous with low TEC (blue).

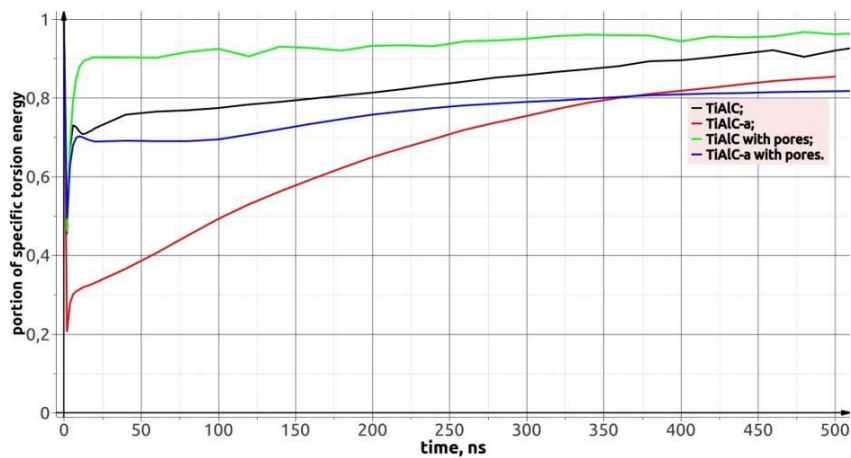


Fig. 8. Time plots of mean **relative latent mechanical energy** for specimens without pores with high TEC (black), without pores with low TEC (red), porous with high TEC (green), porous with low TEC (blue).

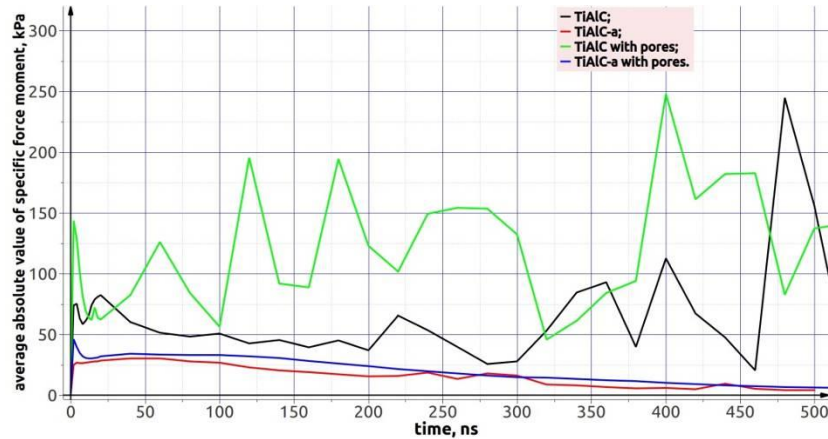


Fig. 9. Time plots of mean **modulus of force moment** for specimens without pores with high TEC (black), without pores with low TEC (red), porous with high TEC (green), porous with low TEC (blue).

The study performed by direct numerical experiment has elucidated that the introduction of the nanoporosity allows appreciably reducing the rate of collective crystallization. It should be noted that the nanoporosity was slowing down the propagation of the heat front in studied modeled specimens. This fact can play both positive and negative role in the process of deposition and further use of a coating. On the one hand, the slowdown of heat front can considerably reduce the level of thermal stresses in deep layers of a material. On the other hand, the slowdown of heat propagation front in the case of high TEC of a material can result in the formation of sharp gradients of thermal stresses that initiate the origination and rapid propagation of a main crack.

In addition, it can be noted that in porous specimens, the rate of collective crystallization was considerably lower than that in nanocrystalline specimens. The study results demonstrate that the value of thermal expansion coefficient has no impact on the rate of recrystallization in nonporous specimens. This means that the driving force in the recrystallization process in this case is primarily the temperature gradient, rather than mechanical stresses.

Figs. 10–13 represent the images of grain structure, distribution of effective stress, modulus of force moment and relative latent mechanical energy in studied specimens at different moments of time.

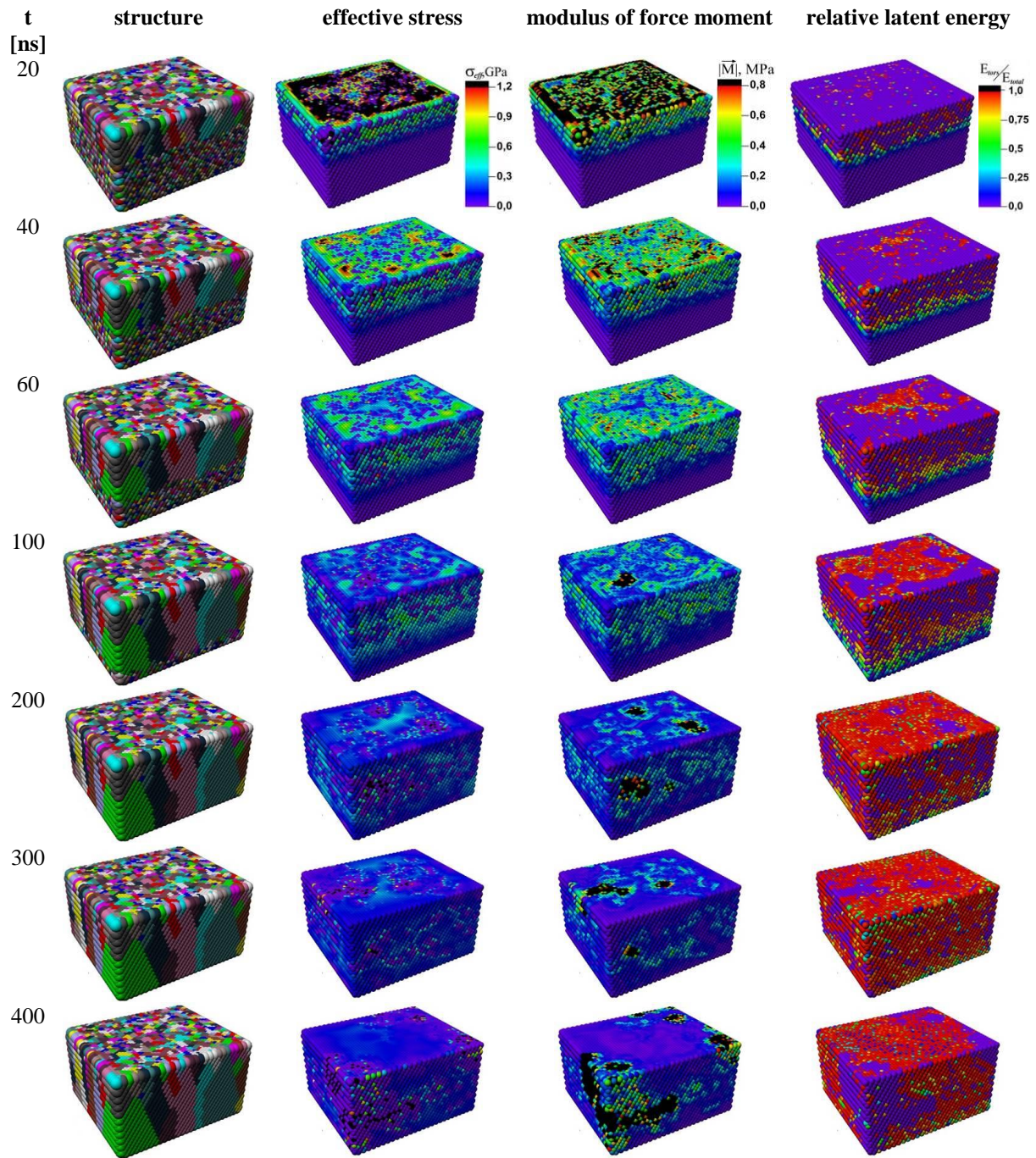


Fig. 10. Images of grain structure, distribution of effective stress, modulus of force moment and relative latent mechanical energy in specimen **without pores and with high TEC** at different moments of time.

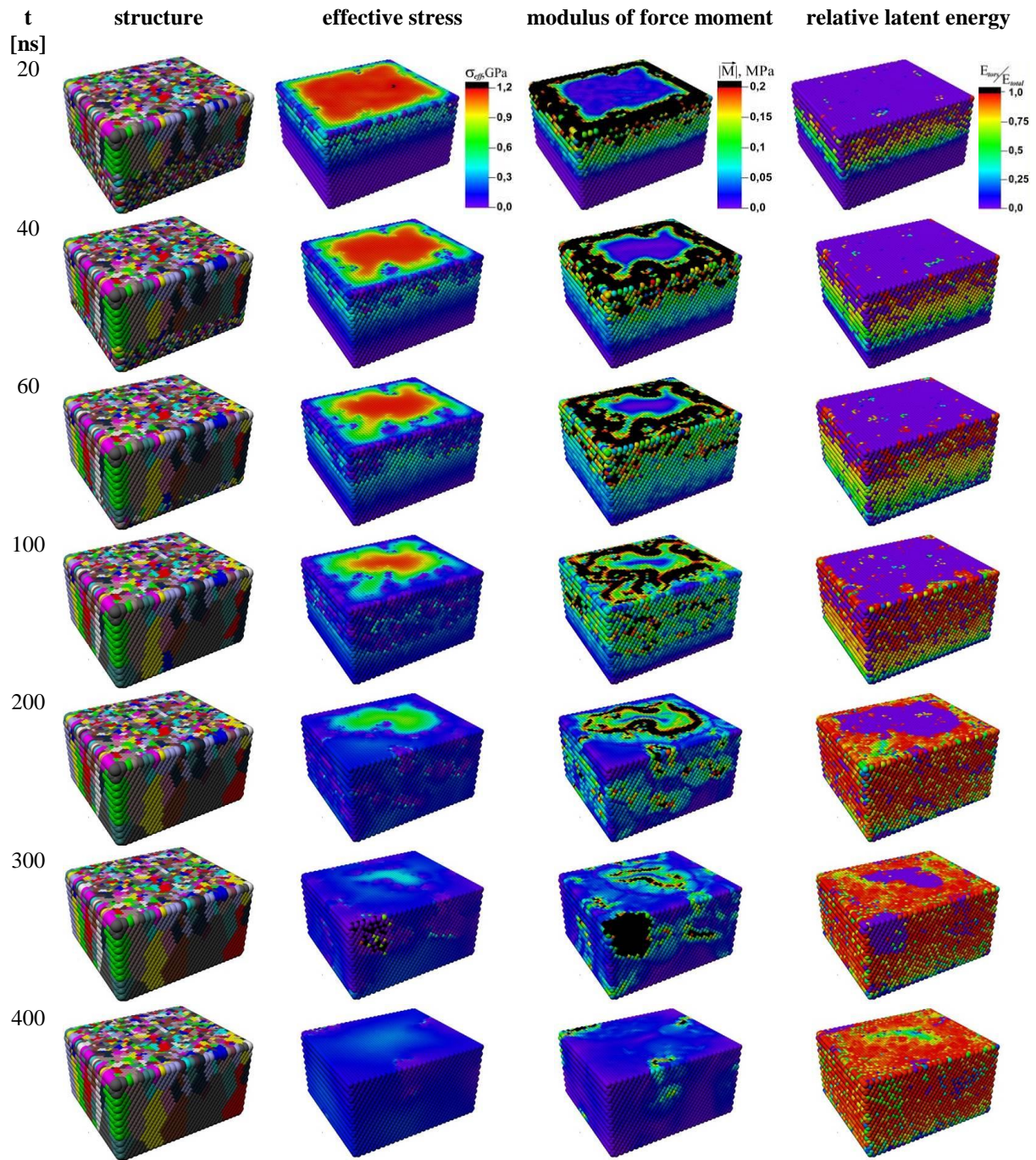


Fig. 11. Images of grain structure, distribution of effective stress, modulus of force moment and relative latent mechanical energy in specimen **without pores and with low TEC** at different moments of time.

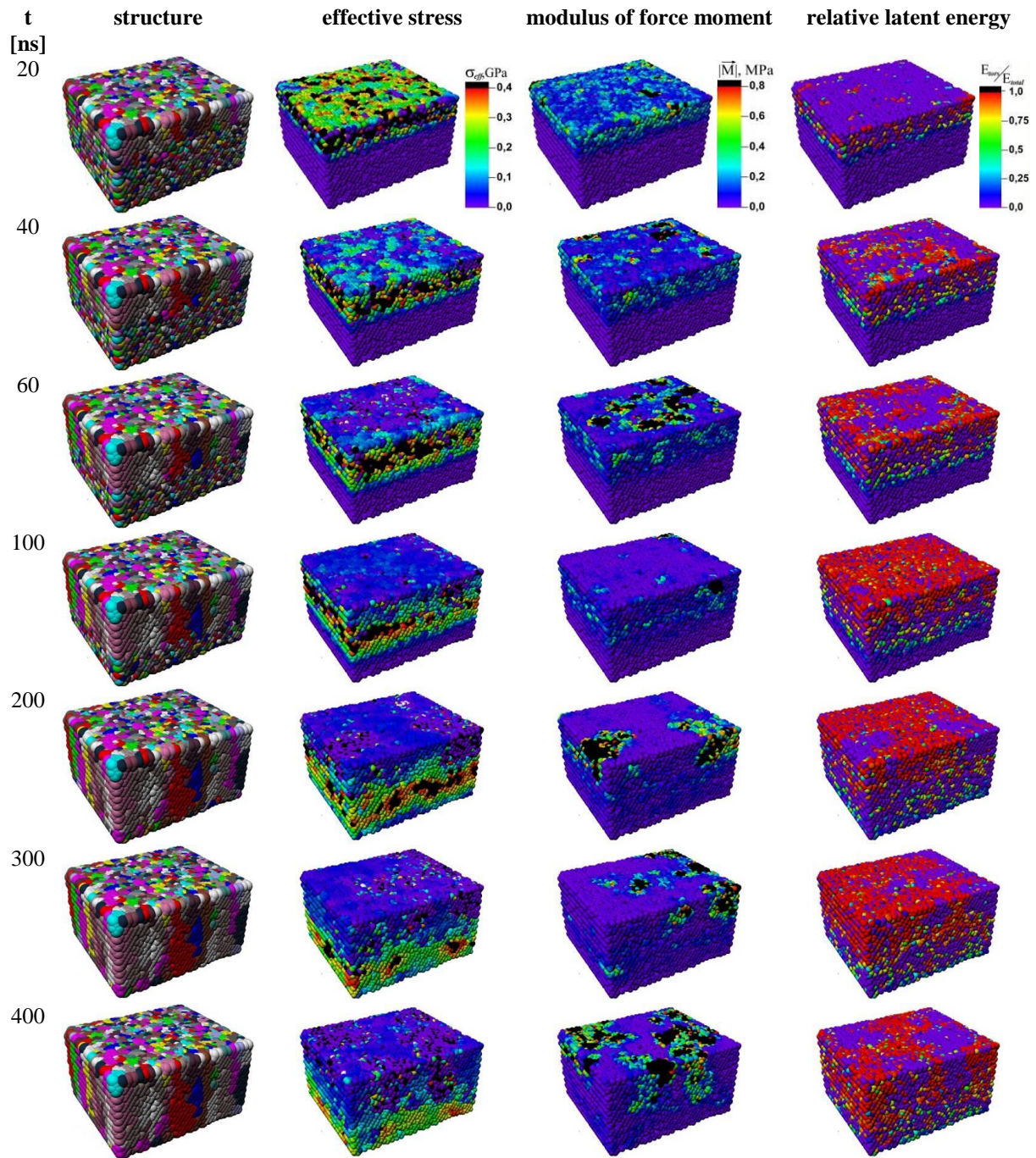


Fig. 12. Images of grain structure, distribution of effective stress, modulus of force moment and relative latent mechanical energy in **porous specimen with high TEC** at different moments of time.

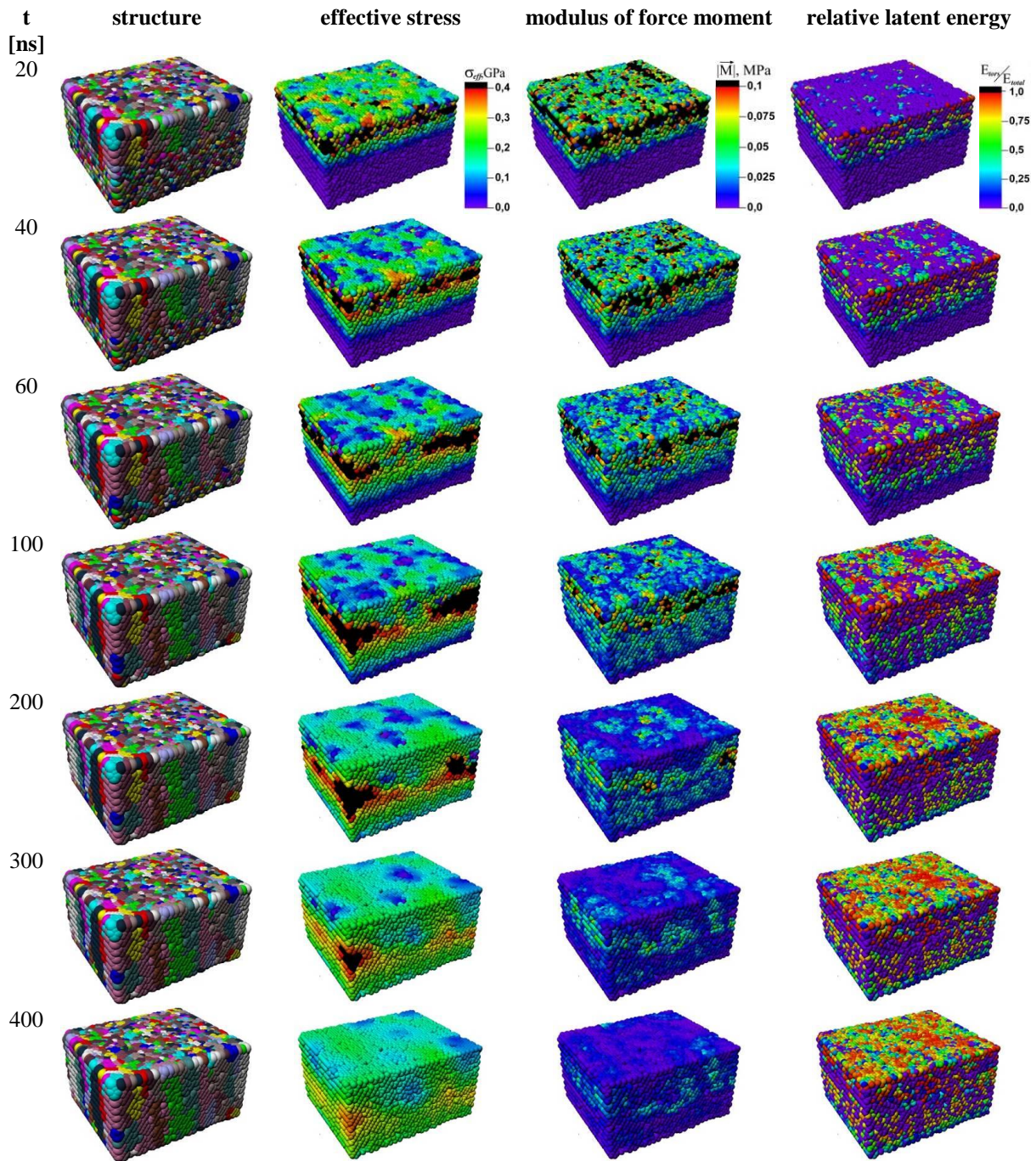


Fig. 13. Images of grain structure, distribution of effective stress, modulus of force moment and relative latent mechanical energy in **porous specimen with low TEC** at different moments of time.

Comparison of the dynamics of defect structure accumulation (Figs. 10–11) and the analysis of plots of relative specific torsion energies (Fig. 8) allows concluding that in nonporous nanocrystalline material, with the decrease of TEC, the rate of defect structure accumulation increases. This fact is explained by the fact that for high values of thermal expansion coefficient, material has higher possibility to relax thermal stresses via three-dimensional deformation without disturbing the translational invariability of the crystal lattice, but increasing the interatomic distance of the latter. In the case of low TEC, the major amount of thermal

stresses transit into local force moments, initiating curvature and torsion of crystal lattice, which unavoidably is accompanied by origination of defect structures at microscale level.

This makes particularly indicative the plots of time dependencies of total modulus of force moment in Fig. 9. Evidently, averaging the modulus of force moment along whole specimen leads at mesoscale level to considerable oscillations of force moment in specimens with high TEC, which testifies elastic rotations of whole conglomerates of grains, which, nevertheless, does not lead to appreciable formation of defect structures in them. The plots of time dependencies of force moments in specimens with low TEC, conversely, are smooth and have 2–4 times lower values.

The comparison of images of defect structure energy distribution both in porous and non-porous specimens shows its more dense and uniform distribution in material with low TEC, while in material with high values of thermal expansion coefficient, the torsion energy is distributed as large areas of its high and low concentration (Figs. 10–13).

This confirms the idea about material with low thermal expansion coefficient achieving larger curvature of crystal lattice at microscale, accompanied by bigger rate of defect structure formation. Such systems rapidly drop stresses into moment forces at microscale impeding the self-organization of rotation moment in large conglomerates of grains.

4 CONCLUSIONS

A new modification of the multiscale hybrid discrete continuum approach of stochastic excitable cellular automata was developed. The new method explicitly accounts for the porosity and nanocrystalline structure of material, the algorithm for computing local force moments and angular velocities of microrotations occurring in structurally nonuniform medium with due account for energy dissipation.

Using the direct numerical experiment it was demonstrated that in porous specimens the rate of collective crystallization was considerably lower than that in nanocrystalline specimens. The study results demonstrate that the value of thermal expansion coefficient has no impact on the rate of recrystallization in nonporous specimens.

On the other hand, the value of thermal expansion coefficient of nanoporous and nanocrystalline specimens significantly impacts the distribution character and rate of defect structure accumulation. For instance, it was shown that the material with low thermal expansion coefficient reaches higher curvature of crystal lattice at microscale. The formation of curvature and torsion in the lattice is accompanied by the formation of defect structures. Such systems are more capable of relaxing moment stresses at microscale, which interferes the self-organization of rotation moment in conglomerates of grains at mesoscale.

Thus, in addition to accounting the local rotational modes of structural elements and thermal radiation by pore walls, it is necessary to study the ability of material to reversible structural transformations in the material of pore walls. The reversible structural transformations will accumulate peak values of energy in elastic rotational stress fields that are knowingly inertial, which will allow preventing catastrophic growth of main cracks.

ACKNOWLEDGEMENTS

The study was conducted under support of fundamental Research Program of Russian State Academies of Sciences for 2013-2020, RFBR projects Nos. 14-01-00789, 14-01-92005 and 15-08-05818 as well as grant of the President of the Russian Federation for support of leading scientific schools No. NSh-2817.2014.1.

REFERENCES

- [1] M. Radovic, M. Barsoum, MAX phases: Bridging the gap between metals and ceramics. *American Ceramic Society Bulletin*, **92**, 20-27, 2013
- [2] E. Levashov, A. Merzhanov, D. Shtansky, Advanced Technologies, Materials and Coatings Developed in Scientific-Educational Center of SHS. *Galvanotechnik*, **9**, 1-13, 2009
- [3] J.P. Lin, L.L. Zhao, G.Y. Li et al., Effect of Nb on oxidation behavior of high Nb containing TiAl alloys. *Intermetallics*, **19**, 131-136, 2001
- [4] A. A. Voevodin, J.S. Zabinski, Nanocomposite and nanostructured tribological materials for space applications. *Composites Science and Technology*, **65**, 741-748, 2006
- [5] A.V. Kartavykh, S.D. Kaloshkin, V.V. Cherdynstev et. al., Application of microstructured intermetallides in turbine manufacture. Part 1: Present state and prospects (a review). *Inorganic Materials: Applied Research*, **4**, 12-20, 2013
- [6] A. A. Voevodin, J. S. Zabinski, C. Muratore, Recent Advances in Hard, Tough, and Low Friction Nanocomposite Coatings. *Tsinghua Science and Technology*, **10**, 665-679, 2005
- [7] D. Shtansky, Ph. Kiryukhantsev-Korneev, A. Sheveyko et. al., Comparative investigation of TiAlC(N), TiCrAlC(N), and CrAlC(N) coatings deposited by sputtering of MAX-phase Ti_{2-x}Cr_xAlC targets. *Surface & Coatings Technology*, **203**, 3595-3609, 2009
- [8] J. Pearson, M. Zikry, K. Wahl, Microstructural modeling of adaptive nanocomposite coatings for durability and wear. *Wear*, **266**, 1003-1012, 2009
- [9] F. Appel, J.-D. Heaton, Gamma Titanium Aluminide Alloys: Science and Technology. Wiley-VCH, 2011
- [10] G. Ying, X. Wang, Numerical Simulation of the SHS Temperature Fields of Al-Ti-C System Based on Plane Propagating Pattern. *Int. J. Mod. Phys. C*, **20**, 1087, 2009
- [11] G. Ying, X. He, S.-Y. Du et al., Kinetics and numerical simulation of self-propagating high-temperature synthesis in Ti-Cr-Al-C systems. *Rare Metals*, **33**, 527-533, 2014
- [12] V.E. Panin, Physical Mesomechanics of Heterogeneous Media and Computer-Aided Design of Materials, Camb. Internat. Science Publ., 1998.
- [13] V.E. Panin, V.E. Egorushkin, Curvature solitons as generalized structural wave carriers of plastic deformation and fracture. *Phys. Mesomech.*, **16**, 267-286, 2013
- [14] Yu.I. Meshcheryakov, T.A. Khantuleva, Nonequilibrium processes in condensed media: Part 1. Experimental studies in light of nonlocal transport theory. *Phys. Mesomech.*, **18**, 228-243, 2015
- [15] J.Kroc, Application of cellular automata simulations to modelling of dynamic recrystallization. *Lecture Notes in Computer Science*, **2329**, 773-782, 2002.
- [16] A. Godara, D. Raabe, Mesoscale simulation of the kinetics and topology of spherulite growth during crystallization of isotactic polypropylen (iPP) by using a cellular automaton. *Modelling Simulation Materials Science Engineering*, **13**, 733-751, 2005.
- [17] F.J. Humphreys, M. Hatherly, *Recrystallization and Related Annealing Phenomena*, Pergamon, New York, 1995.

- [18] D.D. Moiseenko, V.E. Panin, P.V. Maksimov, S.V. Panin, F. Berto, Material fragmentation as dissipative process of micro rotation sequence formation: hybrid model of excitable cellular automata. *AIP Conference Proceedings*, **1623**, 427–430, 2014.
- [19] D.D. Moiseenko, V.E. Panin, T.F. Elsukova, Role of Local Curvature in Grain Boundary Sliding in a Deformed Polycrystal. *Phys. Mesomech.*, **16**, 335-347 , 2013.
- [20] V.E. Panin, V.E. Egorushkin, D.D. Moiseenko et al., Functional role of polycrystal grain boundaries and interfaces in micromechanics of metal ceramic composites under loading. *Computational Materials Science*, **116**, 74-81, 2016